AD-A077 019 ATMOSPHERIC SCIENCE ASSOCIATES BEDFORD MASS F/G 1/4
AIRFLOW EFFECTS ON RIMING MEASUREMENTS BY A WING TIP-MOUNTED IC--ETC(U
AUG 79 H G NORMENT F19628-79-M-0006
UNCLASSIFIED AFGL-TR-79-0194 NL

1 OF 1
AD
A077019

END
DATE
FILMED
12-79
DDC

(18) (19) AFGL-TR-79-0194

LEVEL II

(12)

(6) AIRFLOW EFFECTS ON RIMING MEASUREMENTS BY A WING TIP-MOUNTED ICE DETECTOR ON THE MC130E RESEARCH AIRPLANE.

(10) Hillyer G. Norment

Atmospheric Science Associates
363 Great Road
P. O. Box 307
Bedford, Massachusetts 01730

(11) 24 August 1979

(12) 40

(9) Final Report,
1 Mar [illegible] — 31 August 1979

Approved for public release; distribution unlimited

(15) F19628-79-M-0006

(16) 667Ø

(17) 1Ø

AIR FORCE GEOPHYSICS LABORATORY
AIR FORCE SYSTEMS COMMAND
UNITED STATES AIR FORCE
HANSCOM AFB, MASSACHUSETTS 01731

392 152

Unclassified

SECURITY CLASSIFICATION OF THIS PAGE (When Data Entered)

REPORT DOCUMENTATION PAGE		READ INSTRUCTIONS BEFORE COMPLETING FORM
1. REPORT NUMBER AFGL-TR-79-0194	2. GOVT ACCESSION NO.	3. RECIPIENT'S CATALOG NUMBER
4. TITLE (and Subtitle) AIRFLOW EFFECTS ON RIMING MEASUREMENTS BY A WING TIP-MOUNTED ICE DETECTOR ON THE MC130E RESEARCH AIRPLANE		5. TYPE OF REPORT & PERIOD COVERED 1 March 1979 - 31 August 1979 Final 6. PERFORMING ORG. REPORT NUMBER
7. AUTHOR(s) Hillyer G. Norment		8. CONTRACT OR GRANT NUMBER(s) F19628-79-M-0006 new
9. PERFORMING ORGANIZATION NAME AND ADDRESS ATMOSPHERIC SCIENCE ASSOCIATES 363 Great Road, P.O. Box 307 Bedford, Massachusetts 01730		10. PROGRAM ELEMENT, PROJECT, TASK AREA & WORK UNIT NUMBERS 62101F 667010-06
11. CONTROLLING OFFICE NAME AND ADDRESS Air Force Geophysics Laboratory (LYC) Hanscom AFB, Massachusetts 01731 Contract Manager: Mr. Morton Glass		12. REPORT DATE 24 August 1979 13. NUMBER OF PAGES 40
14. MONITORING AGENCY NAME & ADDRESS(if different from Controlling Office)		15. SECURITY CLASS. (of this report) Unclassified 15a. DECLASSIFICATION/DOWNGRADING SCHEDULE

16. DISTRIBUTION STATEMENT (of this Report)

Approved for public release; distribution unlimited

17. DISTRIBUTION STATEMENT (of the abstract entered in Block 20, if different from Report)

18. SUPPLEMENTARY NOTES

19. KEY WORDS (Continue on reverse side if necessary and identify by block number)

aircraft icing	research aircraft
icing	MC130E
riming	ice indicator
icing measurement	wing tip mounted ice detector

20. ABSTRACT (Continue on reverse side if necessary and identify by block number)

Sampling efficiencies for water drops in the diameter range 10 to 7000 (μm) microns are calculated theoretically at four proposed mounting sites for an icing indicator instrument on the wing tip of the AFGL MC130E airplane. Significant flux distortion of droplets in the diameter range 10 to 100 μm microns is indicated at all four sites. Sensitivity to angle-of-attack of the airplane also is found, and a nose-up angle-of-attack of at least 4° deg is recommended. Additional separation of the sensor probe from the wing tip

DD FORM 1 JAN 73 1473 EDITION OF 1 NOV 65 IS OBSOLETE

Unclassified

SECURITY CLASSIFICATION OF THIS PAGE (When Data Entered)

surface of as little as one-half inch is indicated to substantially ameliorate the sampling problems.

To obtain the sampling efficiencies, trajectories were calculated with use of a three-dimensional flow code that ignores effects of lift vorticity. Exploratory calculations with a similar code that includes lift indicate that the results obtained with the non-lifting flow are optimistic.

ACKNOWLEDGEMENT

The author acknowledges support and assistance by Morton Glass, Arnold Barnes and Hugh Sweeney of the Meteorology Division, AFGL.

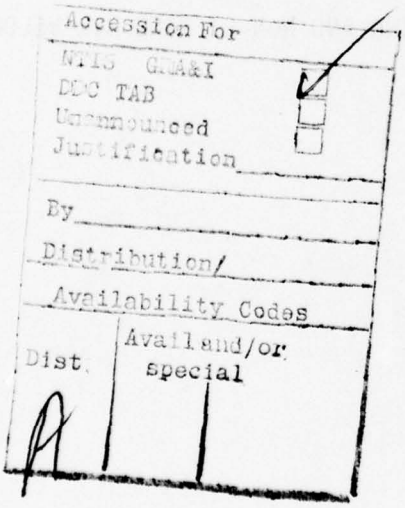

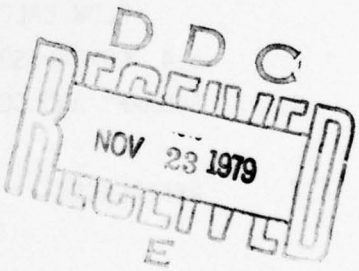

TABLE OF CONTENTS

SECTION		PAGE
1.	INTRODUCTION	5
2.	DESCRIPTION OF THE INSTRUMENT AND ITS MOUNTING LOCATION	6
3.	SAMPLING EFFICIENCY CALCULATIONS	10
	3.1 SHADOWING AND FLUX DISTORTION	10
	3.2 CONCENTRATION FACTOR	11
	3.3 PARTICLE TRAJECTORY CALCULATION	11
	3.4 THREE-DIMENSIONAL FLOW CALCULATION	14
	3.5 PARTICLE DRAG COEFFICIENT	15
4.	CONCENTRATION FACTOR RESULTS	18
	4.1 FLIGHT CONDITIONS	18
	4.2 DIGITAL DESCRIPTION OF THE WING AND WING TIP	18
	4.3 CONCENTRATION FACTORS	18
5.	FLOW CALCULATIONS INCLUDING LIFT EFFECTS	27
	5.1 BASICS	27
	5.2 THE HESS FLOW CODE FOR THREE-DIMENSIONAL LIFTING BODIES	28
	5.3 DIGITAL DESCRIPTION OF THE MC130E WING FOR LIFTING FLOW CALCULATIONS	29
	5.4 COMPARISONS OF LIFTING AND NON-LIFTING AIR VELOCITIES	32
6.	SUMMARY AND CONCLUSIONS	36
7.	REFERENCES	37

LIST OF FIGURES

Figure Number		Page
1.	Dimensioned drawing of the Rosemount Model 871FA ice detector.	6
2.	Plan view of wing and wing tip undersurface showing the four proposed instrument mounting positions.	7
3.	Computer-drawn perspective view of the under side of the wing tip showing the four proposed instrument mounting positions.	9
4.	Trajectories of 100 μm diameter water drops in potential airflow about a prolate ellipsoid of fineness ratio 2.	10
5.	Perspective view of a water drop flux tube.	12
6.	Digital description of the MC130E outer wing and wing tip as used for the concentration factor calculations.	16
7.	Concentration factor vs. water drop diameter at the sensor probe centers at the four proposed mounting sites.	22
8.	Concentration factor vs. water drop diameter for 2° angle-of-attack at the sensor probe center, and at two increased distances from the wing tip surface along the probe axis, both for 4° angle-of-attack.	23
9.	Perspective views of five-trajectory flux tubes of 50 μm diameter water droplets to the center of the sensor probe at proposed mounting site no. 1.	24
10.	Perspective views of five-trajectory flux tubes of 5000 μm diameter water drops to the center of the sensor probe at proposed mounting site no. 1.	25
11.	A wing section with trailing vortex sheet.	27
12.	The generation of streamwise vorticity downstream from a wing due to flow round the ends of the wing from the lower high-pressure side to the upper 'suction' side.	27
13.	Upward curling of the vortex sheet edges to form the wing tip vortices.	28
14.	Digital description of the MC130E half wing used for the lifting flow velocity calculations.	30
15.	Digital description of the MC130E whole wing used for the lifting flow velocity calculations.	31
16.	Relationship of 50 μm diameter droplet trajectory to the MC130E outer wing in plan view.	34

LIST OF TABLES

Table Number		Page
1	COORDINATES FOR THE PROPOSED INSTRUMENT SITES	8
2	CONCENTRATION FACTOR VARIATION WITH WATER DROP DIAMETER AND MOUNTING SITE	20
3	CONCENTRATION FACTOR VARIATION WITH ANGLE OF ATTACK AND DISTANCE ALONG THE SENSOR PROBE AXIS AT MOUNTING SITE 1	21
4	COMPARISON OF LIFTING AND NON-LIFTING AIR FLOW VELOCITIES	33

1. INTRODUCTION

As part of a program to study aircraft icing the Meteorology Division of the Air Force Geophysics Laboratory will measure riming rates aloft via use of a commercially available ice detector mounted on the wing tip of their MC130E research airplane. Several available mounting sites on the underside of the wing tip have been proposed. Here we examine these sites from the aspect of their suitability to provide access to undistorted samples of cloud water drop concentrations. Three-dimensional flow about the outer wing and wing tip were computed and trajectories of water drops ranging in diameters from 10 to 7000 μm were computed to four measurement sites. Shadowing and flux distortion effects are estimated. These calculations ignore effects on air flow of vorticity, which give the wing its lift. As a first step toward estimating the significance of vorticity effects a three-dimensional flow code with lift vorticity was obtained and some exploratory air flow calculations were done such that comparisons with the non-lifting results can be made. As expected, substantial differences are found.

In the remainder of the report first we describe the ice indicator instrument and its proposed mounting sites. Then we discuss the method used to calculate shadowing and flux distortion. Next we present results obtained with the non-lifting flow calculation. Finally, we describe the lifting air flow calculations, we compare some representative results with those that ignore lift vorticity, and discuss their implications to the water drop flux results.

2. DESCRIPTION OF THE INSTRUMENT AND ITS MOUNTING LOCATION

The ice indicator to be used is the Rosemount Model 871FA which is shown in Figure 1. The sensing element is a ¼" diameter circular cylinder of length one inch which extends from the end of a two-inch-long strut. The sensor and strut comprise the section labeled "heated portion" in the figure. This portion of the instrument projects outward from the wing tip surface, and the sensing probe spans a distance from 2" to 3" from the surface.

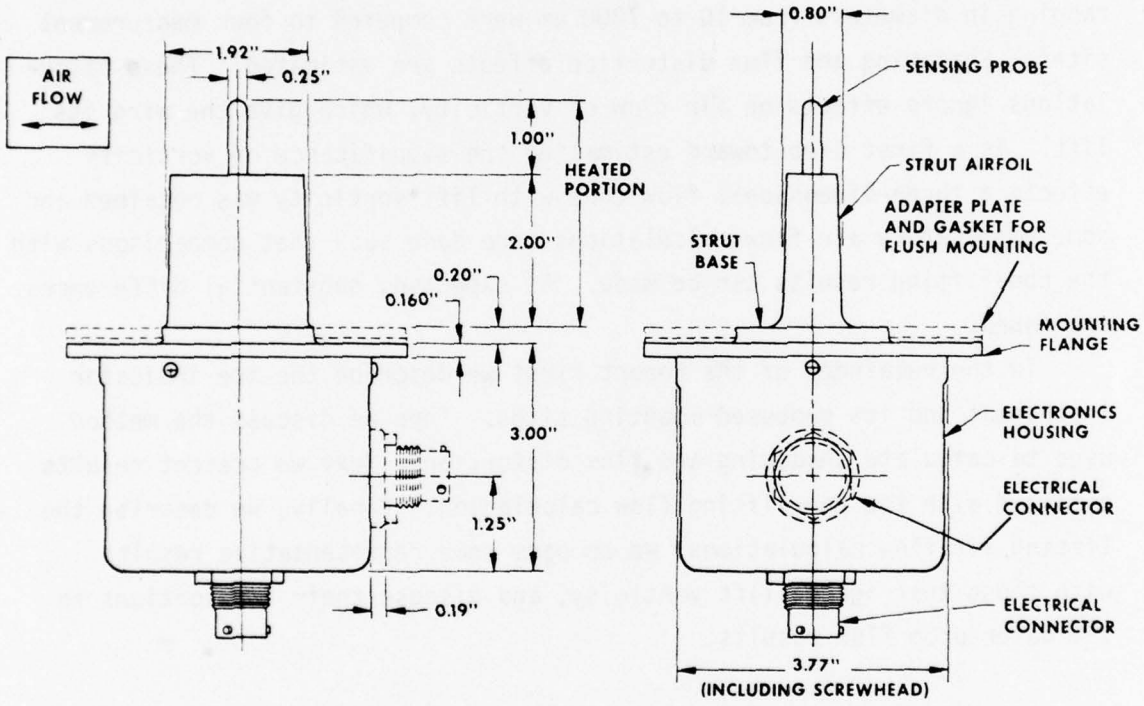

Figure 1. Dimensioned drawing of the Rosemount Model 871FA ice detector.

Figure 2 shows the underside of the outer wing and wingtip with the four proposed mounting sites indicated. Table 1 lists site coordinates. The wingtip begins at the line labeled OWS 562 in Fig. 2. (See Table 1 for the definition of OWS.) Figure 3 shows a computer-drawn perspective plot of a digital description of the wingtip alone; the mounting sites also are marked on this figure.

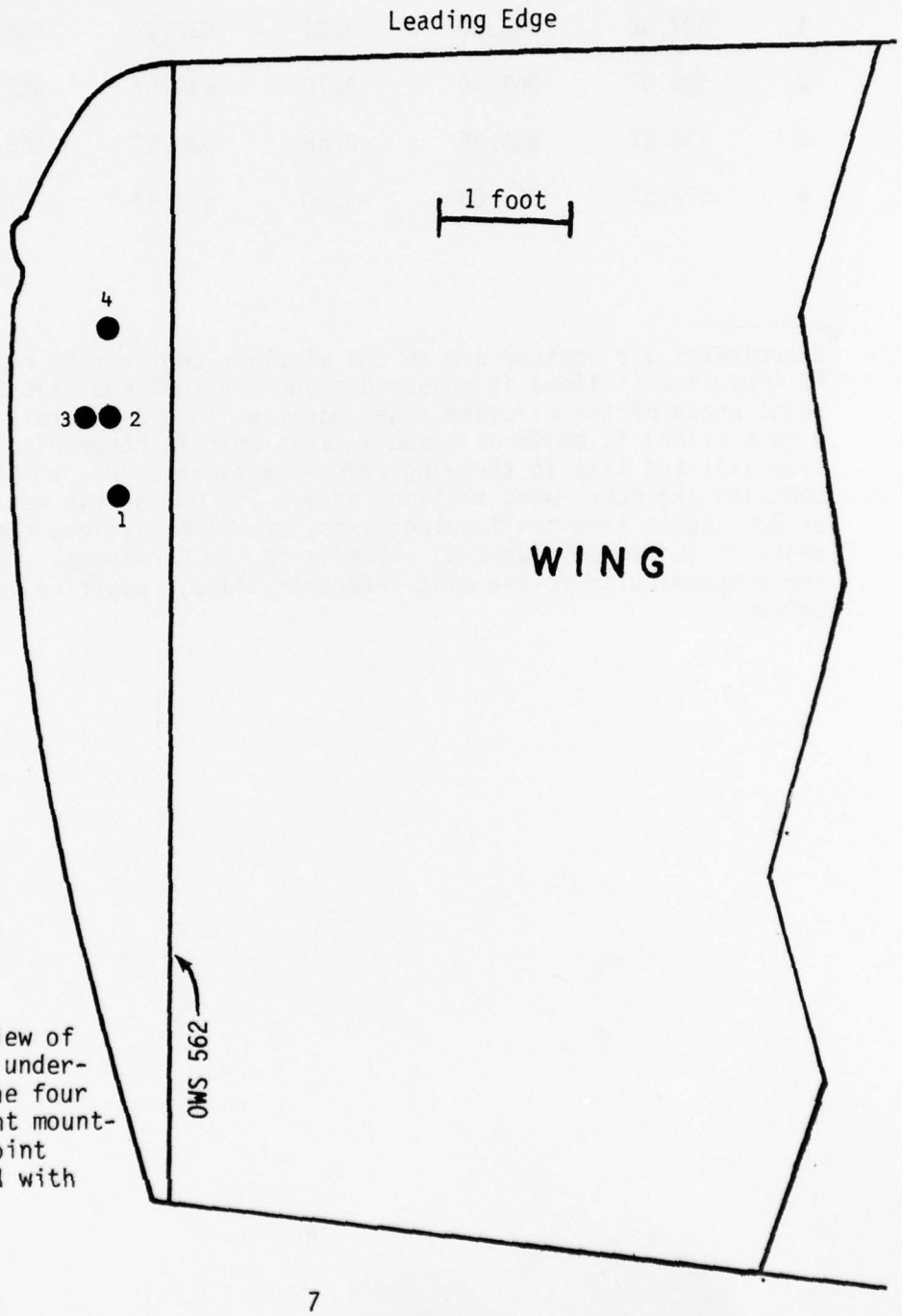

Figure 2. Plan view of wing and wing tip undersurface showing the four proposed instrument mounting positions. Point numbers correspond with those in Table 1.

TABLE 1

COORDINATES* FOR THE PROPOSED INSTRUMENT SITES

	Mounting Point on the Wing Tip Surface			Center of the Sensing Probe		
Site	FS	OWS	WRP	FS	OWS	WRP
1	537.38	566.00	-3.22	537.38	566.42	-5.71
2	530.57	567.00	-3.10	530.57	567.46	-5.54
3	530.57	568.96	-2.66	530.57	569.65	-5.05
4	522.57	567.00	-3.00	522.57	567.45	-5.42

*Coordinates (in inches) are in the airplane engineering reference system: FS (fuselage station) is measured along the fuselage axis from an origin point ahead of the airplane nose, positive toward the tail. OWS (outer wing station) is measured along an axis that is perpendicular to the fuselage axis and lies in the wing reference plane (WRP), which plane also contains the outer wing trailing edge. The OWS origin begins at a distance of 220 inches from the fuselage axis, at which distance the WRP assumes an angle of 2½ degrees (upward) relative to the horizontal. WRP coordinates are perpendicular to the wing reference plane: positive above and negative below.

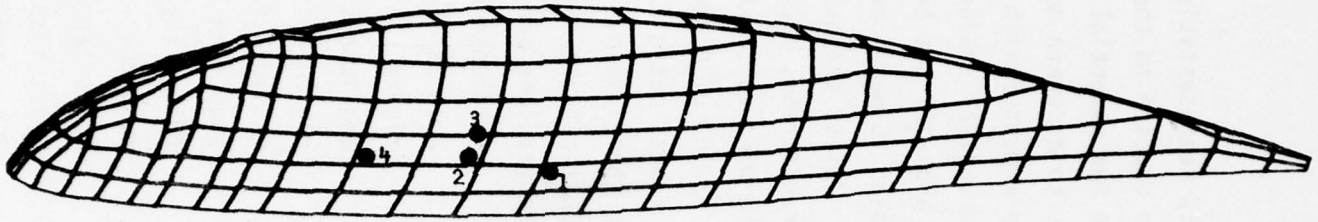

Figure 3. Computer-drawn perspective view of the under side of the wing tip showing the four proposed instrument mounting positions. (The combined wing tip-outer wing as shown in Fig. 6 was used for all concentration factor calculations.)

3. SAMPLING EFFICIENCY CALCULATIONS

3.1 SHADOWING AND FLUX DISTORTION

To measure a riming rate that is representative of free stream cloud conditions, the ice detector must be exposed to the free stream flux of water drops. In this case there are two potential types of shadowing effects that must be considered as obstacles to accurate measurement of free stream icing. These are interation of drop momentum with the curved air flow around the wing tip, and ordinary "umbrella" shadowing. Umbrella shadowing is not found to be significant here and will not be discussed further.

The ice detector sensor is exposed to water drop flux through a small space adjacent to the wing surface. Unless the sampling space is distant enough from the wing to be in the free stream, particles of certain sizes will interact with the flow about the wing to cause flux distortion. The situation is illustrated in Fig. 2 for 100 μm diameter water drops in airflow about a prolate ellipsoid of fineness ratio 2. Note the impaction on the ellipsoid of the drop closest to the ellipsoid symmetry axis, and note the substantial deflections of the next closest trajectories. Trajectory deflection causes high particle concentrations and high concentration gradients to be observed at a point such as the one marked ⊗ 1 in the figure. At point ⊗ 2, deflection and impaction combine to produce a region void of particles, a so-called "shadow zone". Smaller drops, with much less inertia, tend to follow the air flow more exactly such that less distortion is observed. Drops large enough to have very high inertia substantially ignore the air flow, and again little distortion is observed. Therefore, distortion is significant over a limited range of particle sizes.

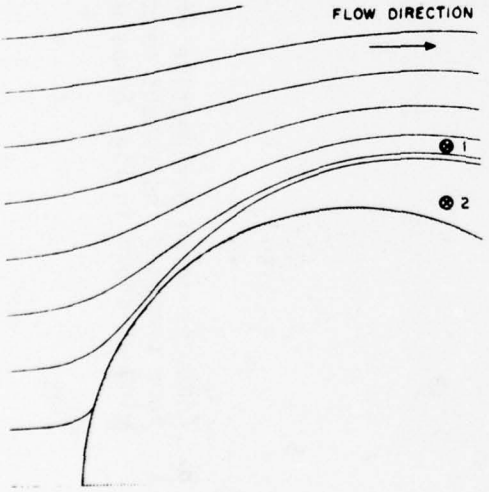

Figure 4. Trajectories of 100 μm diameter water drops in potential airflow about a prolate ellipsoid of fineness ratio 2. (The ordinate scale is expanded by a factor of 2.)

3.2 CONCENTRATION FACTOR

To calculate sampling efficiency, we develop a digital description of the wing and wingtip and use this to calculate air flow around it for specified flight conditions. Then we compute trajectories of hydrometeors through the three-dimensional flow field from the undisturbed cloud to the instrument sensor such as to define a quantity called concentration factor.[1,2,3]

Concentration factor, C_F, is defined as the ratio of particle flux at the sampling or target point, F_t, to the particle flux in the free stream, F,

$$C_F \equiv \frac{F_t}{F} \quad . \tag{1}$$

It is determined by computing particle trajectories from the free stream (initial plane in Fig. 5) to a small area in the target plane (Fig. 5) that surrounds the target point such as to define a particle flux tube. Since the particle mass transfer rate through the tube is constant at all cross sections, it is easily shown that

$$C_F \simeq \frac{A}{A_t} \quad , \tag{2}$$

where A and A_t are the flux tube cross sectional areas in the free stream and at the target point. In the limit as A and A_t approach zero, eq. (2) becomes exact.

3.3 PARTICLE TRAJECTORY CALCULATION

We assume that the bulk air flow is not perturbed by the particles. Moreover, since particle density is large compared to that of air, we can neglect buoyancy and inertial reaction of the fluid to obtain the three-dimensional, normalized equation

---

1. H. G. Norment and R. G. Zalosh, "Effects of Airplane Flowfields on Hydrometeor Concentration Measurements," AFCRL-TR-74-0602 (6 Dec. 1974) AD-A006 690
2. H. G. Norment, "Effects of Airplane Flowfields on Cloud Water Content Measurements," AFCRL-TR-75-0231 (30 April 1975). AD-A014 807
3. H. G. Norment, "Additional Studies of the Effects of Airplane Flowfields on Hydrometeor Concentration Measurements," AFGL-TR-76-0187 (13 August 1976). AD-A032 311

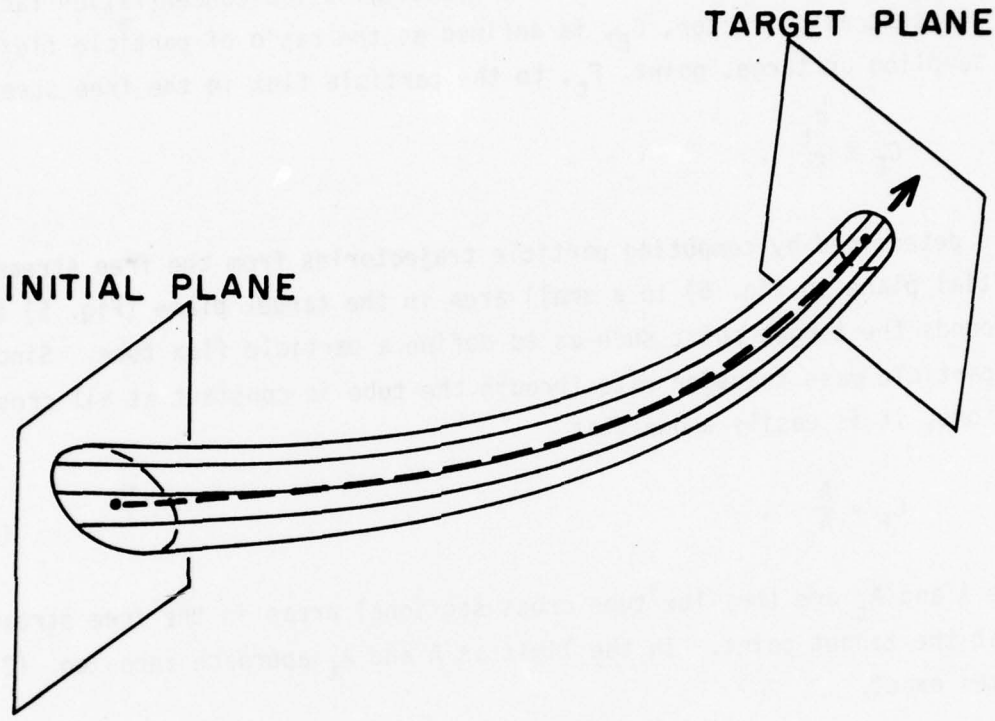

Figure 5. Perspective view of a water drop flux tube. The initial and target planes are perpendicular to the central trajectory (dashed line). Since the peripheral trajectories are constrained to pass through a circle about the central trajectory in the target plane, in general they pass through a non-circular, closed curve in the initial plane.

$$\frac{d\vec{v}_p}{d\tau} = \frac{1}{F_N}\left\{\frac{1}{v_s}(\vec{v}_a - \vec{v}_p)\frac{B_N R_{N,s}}{B_{N,s} R_N} - \vec{k}\right\} \tag{3}$$

Non-dimensioned quantities are:

$\vec{v}_p$, $\vec{v}_a$	particle and air velocities
v_s	still-air terminal settling speed of the particle
$\vec{k}$	unit vector in the z (upward) direction
τ	time
$F_N = V^2/(Lg)$	Froude Number
$R_N = \frac{\rho\delta}{\eta}\left\|\vec{v}_a - \vec{v}_p\right\| V$	Reynolds Number
$B_N = C_D R_N^2$	Davies Number
C_D	particle drag coefficient

Dimensioned quantities are:

δ	particle dimension
ρ	air density
η	air viscosity
g	gravity acceleration constant
V	freestream airspeed
L	a characteristic dimension of the fuselage

Here length is normalized by L, velocity by V and time by L/V. $R_{N,s}$ and $B_{N,s}$ are for still-air, terminal settling of the particles.

Starting at the initial plane, eq. (3) is integrated with respect to time in three-dimensional space via the code DVDQ of Krogh[4] until the target is reached. The method used to compute $\vec{v}_a$ at each time step is described next, and then drag coefficients are discussed.

3.4 THREE-DIMENSIONAL FLOW CALCULATION

In performing concentration factor calculations for sampling sites on particular airplanes, it is important to use three-dimensional airflow. This is the only way to properly account for: airplane geometry and angle-of-attack, airspeed, altitude, and particle settling.

Cloud physics airplanes are subsonic, sampling runs being made typically between 100-150 kts indicated airspeed (IAS). Particle measurement points are beyond the skin-friction boundary layer, and should be placed to avoid regions of separated flow. Therefore, for non-lifting portions of an aircraft, such as the fuselage, potential (i.e., frictionless, incompressible, laminar) flow calculations are quite adequate. For such applications we have used a code developed by Hess and Smith[5,6] for calculating potential flow about arbitrary, non-lifting, three-dimensional bodies. The Hess-Smith code requires input of a digital description of the body surface. This consists of the coordinates of the corner points of a large number of contiguous, plane, quadrilaterals.

Accuracy of the flow calculations has been checked with excellent results by Hess and Smith[5] for many bodies for which analytical solutions are available. Norment and Zalosh[1] have compared computed trajectories around ellipsoids in analytical flow fields with similar trajectories in Hess-Smith flow fields, and they have compared current trajectory results with prior work; agreement is excellent.

---

4. F. T. Krogh, "Variable Order Integrators for Numerical Solutions of Ordinary Differential Equations," Jet Propulsion Lab Technology Utilization Document No. CP-2308 (November 1970).

5. J. L. Hess and A.M.O. Smith, "Calculation of Non-Lifting Potential Flow About Arbitrary Three-Dimensional Bodies," McDonnel Douglas Report E.S. 40622 (15 March 1962). AD-282 255.

6. J. L. Hess and A.M.O. Smith, "Calculation of Potential Flow About Arbitrary Bodies," Progress in Aeronautical Sciences, Vol. 8, edited by D. Kuchemann (Pergammon Press, New York, 1967).

For this case we consider flow around a wing, an obvious lifting body, and use of the non-lifting flow code is suspect. Nevertheless, because of the modest scope of the effort, the pressure of time and the off-the-shelf availability of the non-lifting code, it has been used for the concentration factor calculations. Figure 6 shows a computer plot of the digital description of the MC130E wingtip and outer wing used for this portion of the study.

A more recent version of the flow code, which has capability to compute flow around three-dimensional lifting bodies, was obtained as part of this study and made operational on the AFGL CDC 6600 computer. A digital description of the entire wing was prepared and this was used to obtain selected air flow velocities for comparison with those of the non-lifting code. Details are presented in sec. 5 below.

3.5 PARTICLE DRAG COEFFICIENT

Davies[7] shows that still-air terminal settling of spheres can be generalized in terms of the dimensionless numbers $R_{N,s}$ and $B_{N,s}$. Over the range from the smallest spheres, which settle under viscous flow conditions and obey Stokes law, to spheres much larger than of interest here, and for any Newtonian fluid, a reproducible single-valued relationship between $R_{N,s}$ and $B_{N,s}$ exists. Furthermore, $B_{N,s}$ is independent of settling speed, being a function of fluid and sphere properties only; thus for given sphere and fluid, $R_{N,s}$ can be computed as a function of $B_{N,s}$ were derived by Davies from a composite of many sets of experimental data.

Since the work of Davies, it has been found repeatedly that this treatment is applicable to particles of other shapes, providing settling is steady and particle orientation is stable.

For the trajectory calculations required here, the problem must be turned around. In addition to gravity settling, there is a particle velocity component (relative to air) caused by the disturbance of the passing airplane. At any time step in the numerical integration of eq. (3), $\vec{v}_a - \vec{v}_p$ (and hence R_N) is known, and B_N must be determined. For viscous motion (i.e., Stokes flow, where $R_N < 1$) $B_N = 24\ R_N$ and eq. (3) can be integrated without question. However, for larger R_N the steady-state drag data determined experimentally for terminal settling must be used to compute accelerative particle motion.

---

7. C. N. Davies, "Definitive Equations for the Fluid Resistance of Spheres," Proc. Phys. Soc. (London) 57, 259-270 (1945).

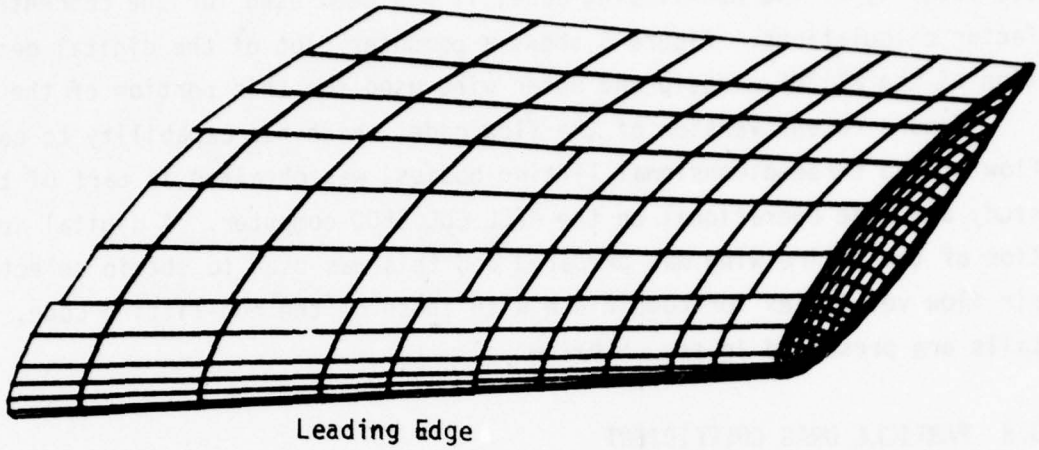

a. Upper surface

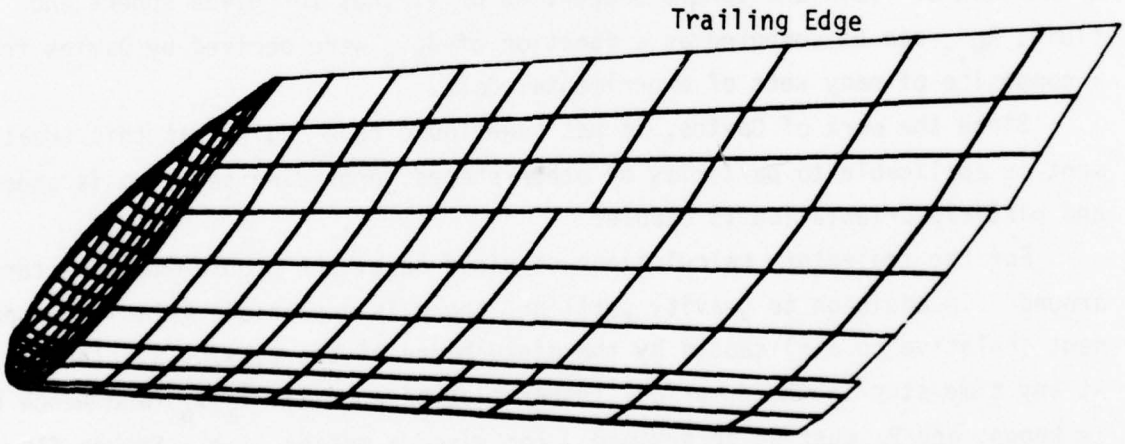

b. Lower surface

Figure 6. Digital description of the MC130E outer wing and wing tip as used for the concentration factor calculations.

Experimental measurements by Keim[8] and a theoretical analysis by Crowe, et al.[9] indicate that if the acceleration modulus,

$$A_N = \delta \left| \frac{dV_p}{dt} \right| / V_p^2 \quad ,$$

is smaller than about 10^{-2}, steady-state drag coefficients can be used without significant error to compute accelerative motion. A_N has never been found to exceed 10^{-2} in our trajectory calculations.

For small water drops, which are spherical, the polynomial equations of Davies[7] are used to compute V_s, while for larger, distorted drops, the equations of Foote and du Toit[10] are used. To compute B_N from R_N, inverse polynomials have been developed, using the data set given by Davies for small drops and Gunn and Kinser[11] for large drops.

---

8. S. R. Keim, "Fluid Resistance to Cylinders in Accelerated Motion," J. Hydraulics Div., Proc. Amer. Soc. Civil Eng., 6, paper 1113 (1956).

9. C. T. Crowe, J. A. Nicholls and R. B. Morrison, "Drag Coefficients of Inert and Burning Particles Accelerating in Gas Streams," Ninth Symp. (Int'l.) on Combustion, Academic Press, pp. 395-405 (1963).

10. G. B. Foote and P. S. du Toit, "Terminal Velocity of Raindrops Aloft," J. Appl. Meteor. 8, 249-253 (1969).

11. R. Gunn and G. D. Kinser, "The Terminal Velocity of Fall for Water Droplets in Stagnant Air," J. Meteor. 6, 243-248 (1949).

4. CONCENTRATION FACTOR RESULTS

4.1 FLIGHT CONDITIONS

All calculations were done for 10 kft altitude and 150 knots indicated airspeed. Using U.S. Standard Atmosphere, 1962 data,[12] we have:

Temperature	268.66°K (-4.49°C)
Pressure	70121 Pa
Density	0.90925 km m^{-3}
True airspeed	91.177 m s^{-1}

A 4°, nose-up angle of attack (AOA) was assumed for all but one set of concentration factor calculations; for the odd set a 2° AOA was used.

4.2 DIGITAL DESCRIPTION OF THE WING AND WING TIP

Figure 3 shows an enlarged view of the digital description of the wing tip alone and Fig. 6 shows the tip combined with the portion of the outer wing used, which extends as far as the inboard end of the aileron. The combined tip and wing section were used for the concentration factor calculations.

Coordinates of points from which the digital description was developed were measured from mold line drawings obtained from the Lockheed Company. With the exception of the aileron mold lines, all of the drawings were full scale; the aileron drawings were approximately half scale. Measurement precision was to about 1 mm, full scale.

The ice indicator instrument was not included in the digital description.

4.3 CONCENTRATION FACTORS

Concentration factors were computed from flux tubes defined by a central trajectory and four peripheral trajectories (Fig. 5). The target plane flux

---

12. S. L. Valley, editor, Handbook of Geophysics and Space Environments, (McGraw-Hill, 1965).

tube radii were 1/6" to within a tolerance of ± 1/12". Effects of the ice indicator probe and supporting strut on the airflow are ignored. Results are listed in Tables 2 and 3 and plotted in Figs. 7 and 8.

Figure 7 shows the results computed for the four mounting sites (Figs. 2 and 3 and Table 1) with the drop flux tube centered at the center of the ice indicator sensing probe at each site (i.e., at a distance of 2½" from the wing tip surface). A 4° angle of attack was assumed for each case. At site 1, which is furthest aft, the possibility of a shadow zone (sec. 3.1) is indicated for droplets in a narrow range of diameters between about 35-45 μm. At the other sites severe flux distortion is indicated; that is, we would expect overestimation of droplet flux, and corresponding enhanced riming, of as much as 35-40% at sites 2 and 3 and about 30% at site 4 for droplets in the narrow range stated above.* For drops larger than about 100 μm and smaller than 10 μm diameters, flux distortion is indicated to be not significant.

Figures 9 and 10 illustrate why there is flux distortion for cloud-sized droplets while there is none for large drops. The small drops follow the flow of air around the wing rather closely; the 50 μm drop trajectories shown in Fig. 9 approach and are deflected by the under side of the leading edge into the high speed flow close to the undersurface of the wing tip. Deflection and particle inertia combine to cause flux tube contraction as described in sec. 3.1. In contrast, large drops which reach the instrument sensor virtually ignore the air flow around the wing as exemplified by the straight-line trajectories of the 5000 μm drops shown in Fig. 10.

The effect of angle-of-attack (AOA) variation is shown by comparison of the upper curves in Figs. 7 and 8 since the differences in these curves are caused solely by decrease in AOA from 4° (Fig. 7) to 2° (Fig. 8). The concentration factor peak is seen to remain stationary with respect to droplet size, but to increase markedly in height and breadth as AOA is decreased. Thus we find marked sensitivity to AOA at site 1, and we can expect similar sensitivity at the other sites.

---

*A concentration factor of unity would indicate that undistorted, free-stream drop fluxes are being seen by the instrument. Values greater than one indicate flux enhancement above free-stream levels. For example, a concentration factor of 1.30 indicates that the drop flux at the target point is 30% higher than in the free stream. A concentration factor curve that rises sharply indicates, for the particle sizes in the sharply rising part, proximity to a shadow zone. (See sec. 3.1 and Fig. 4.)

TABLE 2

CONCENTRATION FACTOR VARIATION WITH WATER DROP DIAMETER AND MOUNTING SITE*

Center of the Sensing Probe
4° Angle-of-Attack

Water Drop Diameter (μm)	Concentration Factor			
	Site 1	Site 2	Site 3	Site 4
8000	.996			
7000		.993	.992	.994
5000	.997	.994	.994	.994
3000	.998	.996	.995	.996
1000	1.005	1.001	1.001	.999
700		1.006	1.005	1.002
500	1.019	1.012	1.008	1.007
300	1.028	1.018	1.014	1.013
100	1.194	1.147	1.144	1.095
80	1.265			
70		1.226	1.220	1.145
50	1.433	1.317	1.323	1.210
30	1.365	1.316	1.294	1.252
10	1.222	1.110	1.106	1.104

*The mounting sites are as shown in Figs. 2 and 3. Coordinates at the center of the sensor probe are given in Table 1.

TABLE 3

CONCENTRATION FACTOR VARIATION WITH ANGLE OF ATTACK
AND DISTANCE ALONG THE SENSOR PROBE AXIS AT MOUNTING SITE 1

Water Drop Diameter (μm)	Concentration Factor		
	Center of Sensor for 2° AOA	Tip of the Sensor	1" From Sensor Tip*
8000	1.023		
7000		.992	.990
5000	1.006	.993	.992
3000	1.000	.994	.994
1000	1.005	1.001	1.000
700	1.013	1.007	1.003
500	1.022	1.016	1.010
300	1.037	1.022	1.032
100	1.252	1.171	1.128
70	1.423	1.250	1.178
50	1.631	1.320	1.211
30	1.433	1.262	1.184
10	1.124	1.109	1.092

*Measured along the sensor probe axis away from the wing tip surface.

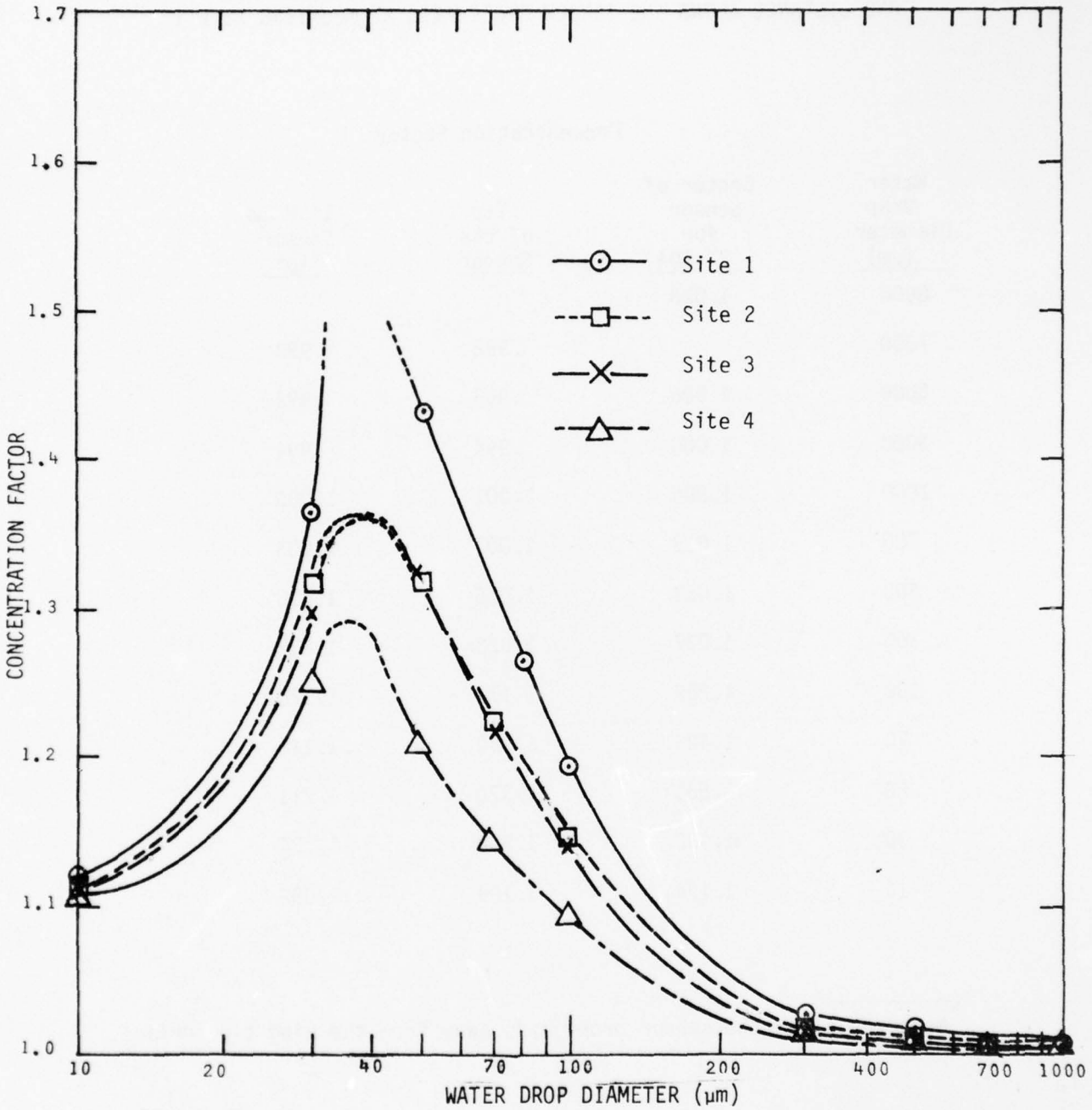

Figure 7. Concentration factor vs. water drop diameter at the sensor probe centers at the four proposed mounting sites. All for 4° angle-of-attack.

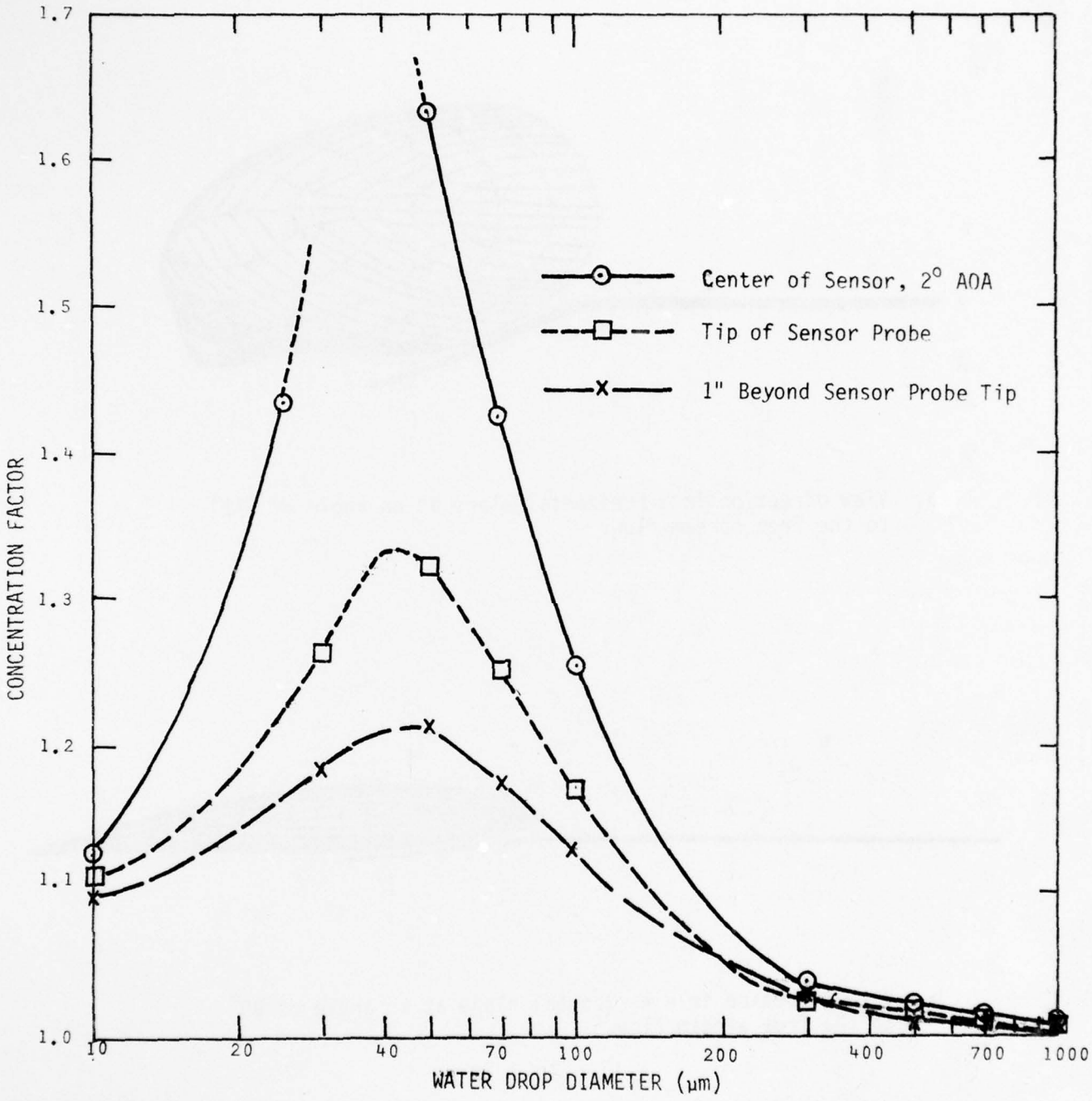

Figure 8. Concentration factor vs. water drop diameter for 2° angle-of-attack at the sensor probe center, and at two increased distances from the wing tip surface along the probe axis, both for 4° angle-of-attack. All for mounting site no. 1.

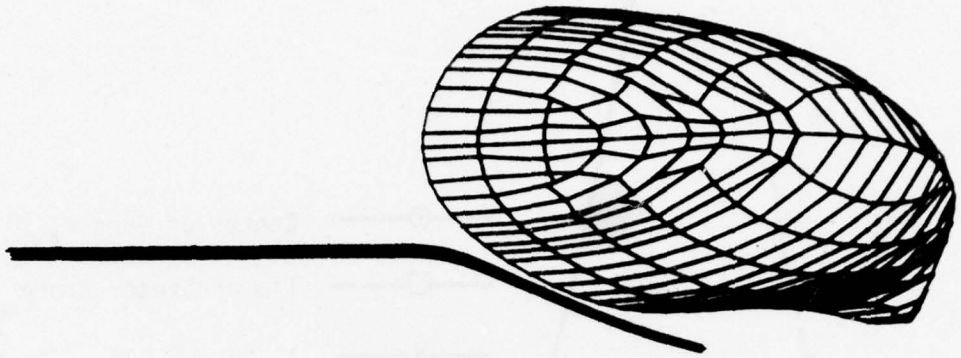

a. View direction in a horizontal plane at an angle of 171° to the free stream flow.

b. View direction in a horizontal plane at an angle of 90° to the free stream flow.

Figure 9. Perspective views of five-trajectory flux tubes of 50 μm diameter water droplets to the center of the sensor probe at proposed mounting site no. 1. 4° angle-of-attack.

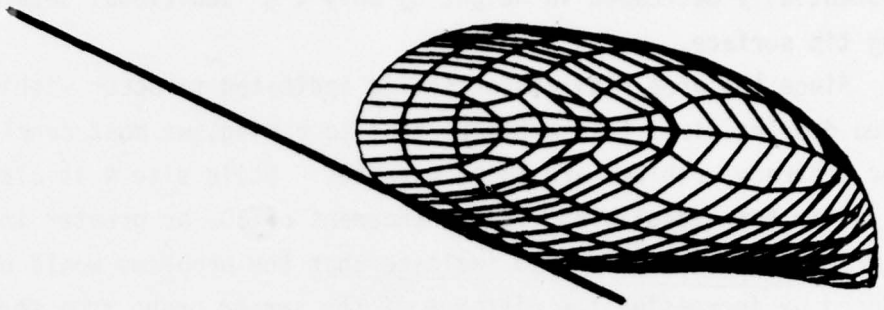

a. View direction in a horizontal plane at an angle of 165° to the free stream flow.

b. View direction in a horizontal plane at an angle of 90° to the free stream flow.

Figure 10. Perspective views of five-trajectory flux tubes of 5000 μm diameter water drops to the center of the sensor probe at proposed mounting site no. 1. 4° angle-of-attack.

Figures 7 and 8 also can be compared to determine the effect of increasing the sensor probe distance from the wing tip surface. Again the concentration factor peak remains stationary with respect to droplet size, but is substantially decreased in height by only a ½" additional separation from the wing tip surface.

Since the drop flux distortion is indicated to occur within a range of cloud droplet sizes that are important to riming, we must conclude that measurement accuracy problems are to be expected. While site 4 is clearly superior, it is far from ideal with flux enhancement of 30% or greater indicated. On the other hand, the results also indicate that the problems would be substantially reduced by increasing the distance of the sensor probe from the wing tip surface by as little as ½ inch. An angle-of-attack of 4^{o} or greater, nose up, during sampling runs is recommended.

As mentioned in sec. 3.4, the results above are suspect because we have ignored vorticity effects (i.e., lift) in the air flow calculations. In the next section we show that these effects are large, and that ignoring them appears to make these concentration factor results optimistic.

5. FLOW CALCULATIONS INCLUDING LIFT EFFECTS

5.1 BASICS

To produce lift, the flows above and below a wing must be different. When these flows recombine at the trailing edge of the wing, their differences persist above and below a thin layer of air that extends indefinitely aftward. The flow velocity gradient across the thin layer produces vorticity, and the thin layer is called a vortex sheet. A section of a wing with its trailing vortex sheet is shown in Fig. 11.

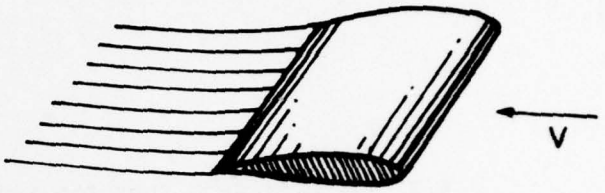

Figure 11. A wing section with trailing vortex sheet.

The geometry of the rotation in the vortex sheet and the way the wing-tip vortices are formed are illustrated by the following model which is taken from Batchelor's book.[13] As is well known, the pressure on the lower surface of a wing is greater than on the upper surface. Owing to this pressure differential there is a tendency for air to flow past the wing tip from the lower toward the upper surface as depicted in Fig. 12. This rotational momentum propagates along the span of the wing, and it is retained by the air after it leaves the trailing edge such as to produce the vortex sheet. The rotation at the wing tip also acts to curl the edges of the vortex sheet to form the so-called wing tip vortices as shown in Fig. 13.

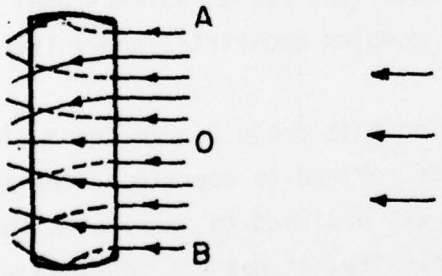

Figure 12. The generation of streamwise vorticity downstream from a wing due to flow round the ends of the wing from the lower high-pressure side to the upper 'suction' side. The trailing vorticity has anti-clockwise sense about the flow direction on the side OA of the wing, and clockwise sense on the side OB.

---

13. G. K. Batchelor, An Introduction to Fluid Dynamics (Cambridge University Press, 1967). Sec. 7.8.

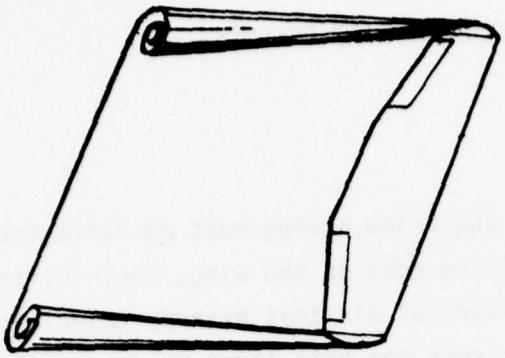

Figure 13. Upward curling of the vortex sheet edges to form the wing tip vortices.

The concentration factor results presented in the preceding section have been calculated with use of an air flow method that does not account for effects of lift vorticity. The questions to be addressed and answered qualitatively in this section are whether the air flow components caused by vorticity would significantly affect drop trajectories, and if so, how they would affect the concentration factor calculations.

5.2 THE HESS FLOW CODE FOR THREE-DIMENSIONAL LIFTING BODIES

John L. Hess has developed a potential flow code for arbitrary three-dimensional lifting bodies that is an extension of the non-lifting code used here for the concentration factor calculations.[14] The code uses a novel method for simulating effects of distributed vorticity via a dipole distribution. Comparison with analytical calculations for two-dimensional airfoils, and with wind tunnel measurements for complex geometries shows that the method produces excellent results.[14]

This code was purchased by AFGL for this project from the National Technical Information Center and it was revised to operate on the AFGL CDC 6600 computer. (As received the code was designed to operate on the IBM 370 computer.) Owing to its size and complexity, it was not possible within the scope of this effort to restructure the code such that it could be used for water drop trajectory calculations as has been done for the non-lifting code.[1] Instead, the code was used in essentially the form received[15] to generate selected air flow velocities for comparison. A digital description of the complete MC130E wing was developed for these calculations.

---

14. J. L. Hess, "Calculation of Potential Flow About Arbitrary Three-Dimensional Lifting Bodies," McDonnell Douglas Report MDCJ5679-01 (October 1972). AD-755 480.

15. D. P. Mack, "Calculation of Potential Flow About Arbitrary Three-Dimensional Lifting Bodies. Users Manual," McDonnell Douglas Report MDCJ5679-02 (October 1972). AD-755 933.

5.3 DIGITAL DESCRIPTION OF THE MC130E WING FOR LIFTING FLOW CALCULATIONS

A second digital description of the MC130E wing, independent of the one described in sec. 4.2 and shown in Fig. 6, was developed for these calculations and is shown in Figs. 14 and 15. The same drawings and procedures were used as before, again to a full-scale measurement precision of approximately 1 mm, but the complete airfoil portion of the wing was described.

On close examination of Figs. 14a and 15a one can see what appears to be an upward curvature in the trailing edge of the wing surface. Actually, the wing trailing edge is defined by the fourth from last spanwise line as indicated in Fig. 14a. Aft of this line, the elements represent the vortex wake adjacent to the trailing edge; the code attaches a semi-infinite wake to the last of these since all vorticity, from the leading edge through the vortex sheet that extends aft to infinity, must be accounted for. Each chordwise strip of lifting elements is defined by 26 elements on the wing plus three wake elements.

The shaded strips of panels shown in Fig. 14b cover the areas under the wing where the engines are mounted. These were treated as "ignored elements" in the calculations; that is, they were not allowed to contribute to lift but were used to maintain vortex distribution continuity along the span of the wing.[14,15] The gap between the two wing sections seen in Fig. 15 is the space occupied by the fuselage. This gap was bridged by "extra strips"[14,15] but the presence of the fuselage was not accounted for in the calculations.

Also ignored in these calculations was the shape and closure of the wing tip. The wing description does not extend outboard beyond OWS 562 into the tip region (see Fig. 2). The code has a special treatment for wing tips whereby it creates a "ficticious logical strip" of lifting elements in the tip area such that the bound vorticity drops to zero at the midspan of the ficticious logical strip. This treatment overrides any other viable specification. This has been found to work satisfactorily and to be insensitive to the width of the ficticious logical strip, but it should be understood that in this application we focus attention on that particular region of the wing where the least accuracy is likely to be found in the flow calculations.

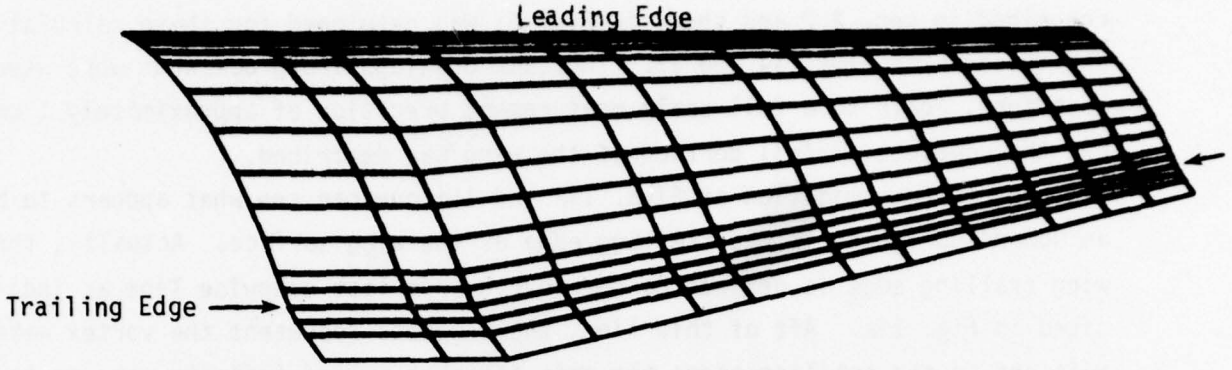

a. Upper surface. Surface elements aft of the trailing edge represent the near-field vortex wake.

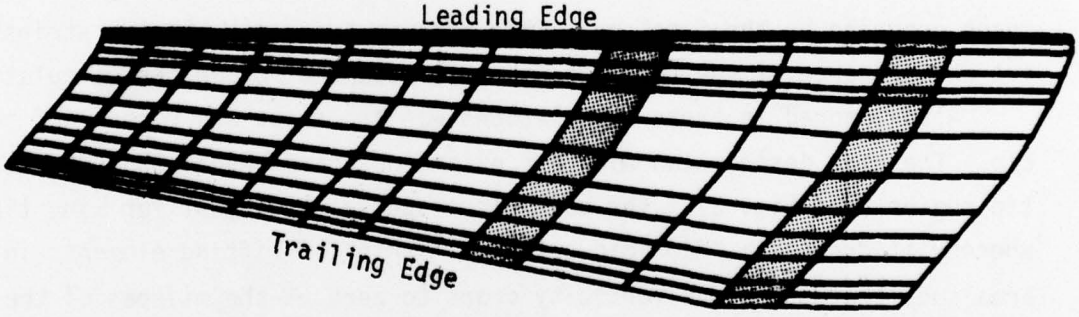

b. Lower surface. Shaded elements cover the areas occupied by the engine mounts.

Figure 14. Digital description of the MC130E half wing used for the lifting flow velocity calculations.

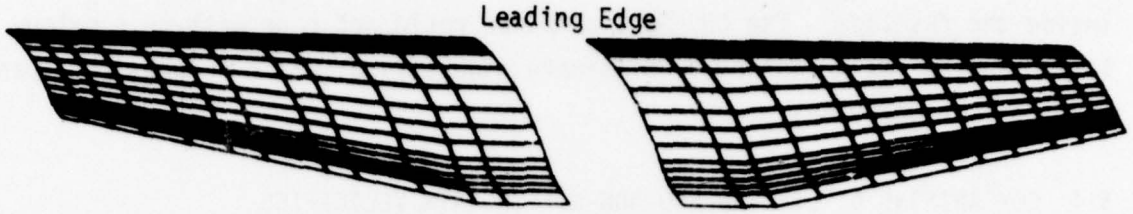

a. Upper surface

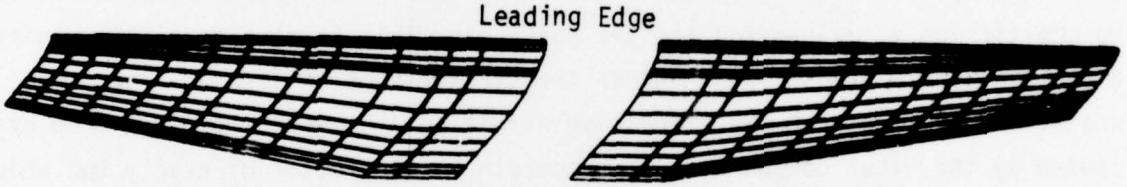

b. Lower surface

Figure 15. Digital description of the MC130E whole wing used for the lifting flow velocity calculations. The central gap is the region occupied by the fuselage.

Another matter of concern is the crude spanwise spatial resolution of the wing digital description. Originally each half wing section was described by 21 chordwise strips of lifting elements plus the "extra strip" at the root inside the fuselage. The CDC 6600 computer could not cope with this calculation and it was necessary to eliminate nine strips, which reduces the spanwise resolution by 41%.

5.4 COMPARISONS OF LIFTING AND NON-LIFTING AIR VELOCITIES

Air velocities calculated by the lifting and non-lifting codes are listed in Table 4. Velocities in Table 4a are for points for which concentration factor results are given in sec. 4.3. Table 4b compares velocities along the trajectory, computed using non-lifting flow, of a 50 μm diameter drop to the center of the sensor probe at mounting site 1. Figure 16 shows the locations of the points along the trajectory.

The significant feature of the data is that for points well under the wing the component in the outboard direction along the spanwise wing axis, v_y, is nearly doubled by including the lift vorticity. As discussed in sec. 5.1 an increase in this component is to be expected, and moreover, this increase would be expected to be greatest at the wing tip. The average ratio of lifting to non-lifting v_y values for the six points in Table 4a plus trajectory points 6 and 7 in Table 4b is 1.83. Though the streamwise flow strongly dominates, whatever deviation from the streamwise direction that occurs for the droplets is caused by the other components, and accordingly the factor of nearly two which distinguishes the lifting from the non-lifting v_y components must be considered significant. The smaller differences in the vertical components, v_z, however, should not be considered significant.

Effects of the v_y difference on concentration factor calculations are impossible to predict with confidence because of the complexity of the geometry and the non-linearity of the mathematics. On the other hand it is clear that inclusion of lift vorticity would cause water drops to traverse longer paths

TABLE 4

COMPARISON OF LIFTING AND NON-LIFTING AIR FLOW VELOCITIES*

a. Selected Locations

Location	Lifting v_x v_y v_z	Non-Lifting v_x v_y v_z	Location	Lifting v_x v_y v_z	Non-Lifting v_x v_y v_z
Site 1, at center of sensor probe	1.0401 .1762 -.0255	1.0761 .0904 -.0237	Site 2, at center of sensor probe	1.0301 .1919 -.0199	1.0699 .0982 -.0322
Site 1, at sensor probe tip	1.0386 .1639 -.0192	1.0729 .0855 -.0153	Site 3, at center of sensor probe	1.0323 .1854 .0297	1.0656 .1072 -.0209
Site 1, 1" outward from sensor probe tip	1.0358 .14611 -.0065	1.0691 .0801 -.0142	Site 4, at center of sensor probe	1.010 .2010 -.0401	1.0580 .1121 -.0568

b. Points on the Trajectory of a 50 μm Diameter Water Drop To the Sensor Probe Center at Mounting Site 1. (See Figure 16 for point locations.)

Point	Lifting v_x v_y v_z	Non-Lifting v_x v_y v_z	Point	Lifting v_x v_y v_z	Non-Lifting v_x v_y v_z
	.998	.998		.928	1.0251
1	.0028	.0012	5	.0748	.1163
	.0170	.0006		-.2344	-.1452
	.997	.997		1.009	1.0597
2	.0040	.0023	6	.1741	.1072
	.0211	.0010		-.1245	-.0722
	.990	.988		1.032	1.0673
3	.0119	.0114	7	.1778	.0972
	.0390	.0035		-.0599	-.0476
	.943	.927		1.040	1.0761
4	.0473	.0543	Site 1	.1762	.0904
	.0651	-.0055		-.0255	-.0237

*Velocity components are orthogonal and are normalized by dividing by the free stream airspeed. v_x and v_y are in the horizontal plane with v_x in the free stream direction and v_y positive in the outboard direction. v_z is positive upward.

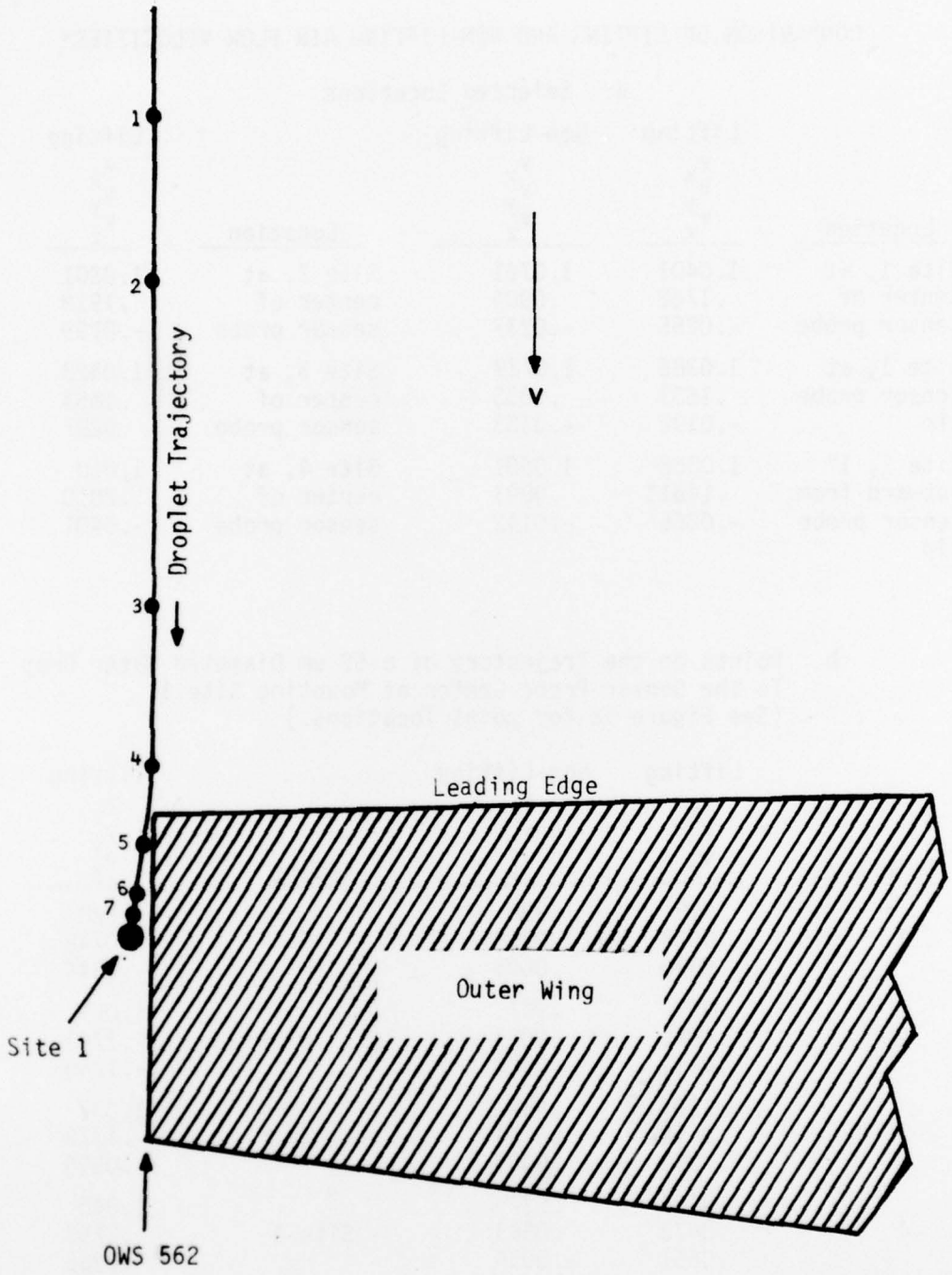

Figure 16. Relationship of 50 μm diameter droplet trajectory to the MC130E outer wing in plan view. The numbered points correspond to those in Table 4b.

under the wing which, according to past experience with fuselage-mounted instruments, causes increase in severity of shadowing and flux distortion. Therefore, these results lead to the conclusion that the concentration factor results reported above are most likely to underestimate riming measurement problems at the four proposed instrument mounting sites.

6. SUMMARY AND CONCLUSIONS

Water drop sampling efficiency has been evaluated theoretically at four proposed instrument mounting sites on the wing tip of an MC130E airplane. Trajectories of water drops ranging in size from 10 μm to 7000 μm in diameter were calculated from the free stream to the instrument sites via use of a three-dimensional flow code that ignores effects of lift vorticity. These calculations indicate that the instrument sensor at the aftmost mounting site may be shaded from droplets in the narrow range of diameters from about 35 to 45 μm. Severe overestimation of droplet flux, and hence riming, by droplets in the range of 10 to 150 μm diameters also is indicated. The mounting site in the most forward location is indicated to be most favorable, but overestimation of droplet flux by as much as 30% is indicated for the same range of droplet sizes. Increase in distance from the wing tip surface of the sensor probe by as little as one-half inch causes a substantial reduction in shadowing and flux overestimation. Marked sensitivity to angle-of-attack is indicated, and an angle-of-attack of not less than about 4°, nose up, is recommended.

To estimate the effect of lift vorticity neglect, air velocities were calculated at selected points by a code which does include lift vorticity. Comparison with velocities used for the trajectory calculations shows that for points at and near the proposed sensor locations, components along the spanwise wing axis in the outboard direction are nearly doubled by including lift effects. This implies that water drops whould have longer traverses under the wing than calculated, which, based on past experience, implies more severe sampling problems than indicated by use of the non-lifting flow.

7. REFERENCES

1. H. G. Norment and R. G. Zalosh, "Effects of Airplane Flowfields on Hydrometeor Concentration Measurements," AFCRL-TR-74-0602 (6 December 1974). AD-A006 690

2. H. G. Norment, "Effects of Airplane Flowfields on Cloud Water Content Measurements," AFCRL-TR-75-0231 (30 April 1975). AD-A014 807

3. H. G. Norment, "Additional Studies of the Effects of Airplane Flowfields on Hydrometeor Concentration Measurements," AFGL-TR-76-0187 (13 August 1976). AD-A032 311

4. F. T. Krogh, "Variable Order Integrators for Numerical Solutions of Ordinary Differential Equations," Jet Propulsion Lab Technology Utilization Document No. CP-2308 (November 1970).

5. J. L. Hess and A.M.O. Smith, "Calculation of Non-Lifting Potential Flow About Arbitrary Three-Dimensional Bodies," McDonnel Douglas Report E.S. 40622 (15 March 1962). AD-282 255

6. J. L. Hess and A.M.O. Smith, "Calculation of Potential Flow About Arbitrary Bodies," Progress in Aeronautical Sciences, Vol. 8, edited by D. Kuchemann (Pergammon Press, New York, 1967).

7. C. N. Davies, "Definitive Equations for the Fluid Resistance of Spheres," Proc. Phys. Soc. (London) 57, 259-270 (1945).

8. S. R. Keim, "Fluid Resistance to Cylinders in Accelerated Motion," J. Hydraulics Div., Proc. Amer. Soc. Civil Eng., 6, paper 1113 (1956).

9. C. T. Crowe, J. A. Nicholls and R. B. Morrison, "Drag Coefficients of Inert and Burning Particles Accelerating in Gas Streams," Ninth Symp. (Int'l.) on Combusion, Academic Press, pp. 395-405 (1963).

10. G. B. Foote and P. S. du Toit, "Terminal Velocity of Raindrops Aloft," J. Appl. Meteor. 8, 249-253 (1969).

11. R. Gunn and G. D. Kinser, "The Terminal Velocity of Fall for Water Droplets in Stagnant Air," J. Meteor. 6, 243-248 (1949).

12. S. L. Valley, editor, Handbook of Geophysics and Space Environments, (McGraw-Hill, 1965).

13. G. K. Batchelor, An Introduction to Fluid Dynamics (Cambridge University Press, 1967). Sec. 7.8.

14. J. L. Hess, "Calculation of Potential Flow About Arbitrary Three-Dimensional Lifting Bodies," McDonnell Douglas Report MDCJ5679-01 (October 1972). AD-755 480.

15. D. P. Mack, "Calculation of Potential Flow About Arbitrary Three-Dimensional Lifting Bodies. User's Manual," McDonnell Douglas Report MDCJ5679-02 (October 1972). AD-755 933.